AD NUMBER

AD857512

LIMITATION CHANGES

TO:

Approved for public release; distribution is unlimited.

FROM:

Distribution authorized to U.S. Gov't. agencies and their contractors; Critical Technology; JUL 1969. Other requests shall be referred to U.S. Army Aberdeen Research and Development Center, Aberdeen Proving Ground, MD. This document contains export-controlled technical data.

AUTHORITY

BRL D/A ltr, 22 Apr 1981

BRL

MEMORANDUM REPORT NO. 1998

AERODYNAMIC PROPERTIES OF THE 152MM XM617 PROJECTILE

by

Fred J. Brandon

July 1969

U.S. ARMY ABERDEEN RESEARCH AND DEVELOPMENT CENTER
BALLISTIC RESEARCH LABORATORIES
ABERDEEN PROVING GROUND, MARYLAND

B A L L I S T I C R E S E A R C H L A B O R A T O R I E S

MEMORANDUM REPORT NO. 1998

JULY 1969

AERODYNAMIC PROPERTIES OF THE 152mm XM617 PROJECTILE

Fred J. Brandon

Exterior Ballistics Laboratory

RDT&E Project No. 1T262301A201

A B E R D E E N P R O V I N G G R O U N D, M A R Y L A N D

B A L L I S T I C R E S E A R C H L A B O R A T O R I E S

MEMORANDUM REPORT NO. 1998

FJBrandon/pp
Aberdeen Proving Ground, Md.
July 1969

AERODYNAMIC PROPERTIES OF THE 152mm XM617 PROJECTILE

ABSTRACT

The results obtained from exterior ballistic tests of the XM617 projectile are presented and discussed. An XM81E12 launcher with a twist of one turn in 41.2 calibers was used. Some real range drag, stability and damping characteristics are also presented and discussed.

TABLE OF CONTENTS

LIST OF ILLUSTRATIONS

LIST OF SYMBOLS

C_D	$= \frac{\text{Drag force}}{1/2\ \rho V^2 S}$	A positive C_D corresponds to a force along the trajectory which is opposing the velocity vector.
C_{M_α}	$= \frac{\text{Static moment}}{1/2\ \rho V^2 S \ell \alpha_t}$	A positive C_{M_α} corresponds to a moment which is acting to increase the total angle of attack.
$C_{M_q} + C_{M_{\dot{\alpha}}}$	$= \frac{\text{Damping moment}}{1/2\ \rho V^2 S \ell \left(\frac{q_t \ell}{V}\right)}$	A positive $C_{M_q} + C_{M_{\dot{\alpha}}}$ corresponds to a moment which is acting to increase the angular velocity.
C_{N_α}	$= \frac{\text{Normal force}}{1/2\ \rho V^2 S \alpha_t}$	A positive C_{N_α} corresponds to a force which is acting to move the missile in the direction of the total angle of attack.
$C_{M_{p\alpha}}$	$= \frac{\text{Magnus moment}}{1/2\ \rho V^2 S \ell \left(\frac{p\ell}{V}\right)\alpha_t}$	A positive $C_{M_{p\alpha}}$ corresponds to a moment which is acting to move the missile's nose around the trajectory in the direction of spin.
$\overline{\delta^2}$	mean squared yaw	
α_t	total angle of attack	
ρ	air density	
S	$\frac{\pi d^2}{4}$	
d	body diameter of projectile	
q_t	total angular velocity	
$C_{D_{\overline{\delta^2}}}$	yaw drag coefficient	
C_{D_o}	zero yaw drag coefficient	

LIST OF SYMBOLS (Continued)

$\lambda_{1,2}$	damping rates -- a negative λ_j yields damped motion
$K_{1,2}$	amplitude of nutation or precession yaw vectors
I_x	axial moment of inertia
I_y	transverse moment of inertia
ℓ	reference length (for this report ℓ = d)
M	Mach number
p	rolling velocity

I. INTRODUCTION

Free flight tests of the XM617 projectile were conducted at the Ballistic Research Laboratories' Transonic Range facility[1] to verify the stability of the projectile and to determine its aerodynamic characteristics. The XM617 is a special purpose 152mm projectile (Figure 1) used for relatively short ranges at a standard muzzle velocity near 640 meters per second. The only unusual feature of the projectile is its low weight to volume ratio.

The tests at the Transonic Range facility were conducted using the same gun and tracked carriage that were used to obtain firing table data, thus approximating the same launch conditions. The carriage used was an M551 tracked vehicle with an XM81E12 launcher, tube number 43 (Figure 2). The launch tube is a rifled tube with a right hand twist of one turn in 41.2 calibers. Data were obtained for projectiles fired with the standard velocity and at lower values down to 260 meters per second.

This report contains the results obtained from the tests. The physical properties of the projectile were obtained prior to launch by the method discussed in Reference 2 and are given in Figure 3. The stability and aerodynamic data were processed in the usual manner[3] and are presented in Table 1, and in Figures 10 through 19 which follow in the text.

II. AERODYNAMIC DATA

The aerodynamic force and moment system is inferred by fitting the attitude oscillations and the center of mass oscillations about a mean trajectory of the test shell in its flight along the instrumented range. The results are then dependent on the size and accuracy of measurements of these motions. The XM617 is relatively short compared to

TABLE 1 AERODYNAMIC PROPERTIES OF XM617 PROJECTILES

Rd. No.	M	$\sqrt{\overline{\delta^2}}$ (deg)	C_D	C_{M_α}	$C_{M_q} + C_{M_{\dot\alpha}}$	$C_{M_{p\alpha}}$	C_{N_α}	CP_N (cal. from base)	$10^3 \lambda_1$ (1/cal)	$10^3 \lambda_2$ (1/cal)	s_g	K_1 (rad)	K_2 (rad)
2-8365	1.831	5.0	.458	1.10	-2.7	.04	2.84	1.48	-.59	-.20	1.97	.056	.072
2-8366	1.128	1.9	.583	1.16	-2.2	-.01	2.90	1.49	-.52	-.16	1.98	.018	.027
2-8367	1.269	2.0	.528	1.20	-4.3	.42	2.77	1.52	-.56	-.54	1.83	.023	.028
2-8368	1.255	2.6	.540	1.15	-4.0	.24	2.76	1.50	-.69	-.34	1.80	.026	.035
2-8369	1.135	2.5	.595	1.09	-4.1	.31	2.80	1.48	-.62	-.42	2.06	.024	.034
2-8370	1.003	0.6	.520	1.30	-6.0	.60	3.45	1.46	-.77	-.74	1.64	.007	.005
2-8371	1.002	0.9	.519	1.25	-1.9	.24	2.90	1.52	-.16	-.47	1.72	.005	.015
2-8372	.924	1.6	.287	1.54	-1.7	.18	2.10	1.82	-.17	-.36	1.36	.026	.013
2-8373	.925	1.7	.289	1.52	-2.4	.19	1.88	1.90	-.37	-.28	1.38	.016	.024
2-8374	1.533	3.1	.474	1.14	-3.8	.16	2.68	1.51	-.74	-.26	1.93	.031	.043
2-8375	1.542	5.4	.514	1.11	-2.7	.07	2.80	1.49	-.55	-.22	1.98	.050	.078
2-8376	.793	2.7	.235	1.44	-1.4	.03	2.13	1.76	-.28	-.18	1.44	.022	.041
2-8377	.784	2.0	.230	1.41	-2.0	-.02	2.36	1.69	-.53	-.08	1.46	.013	.032
2-8378	1.812	5.7	.464	1.09	-2.8	.09	2.77	1.48	-.53	-.24	2.02	.058	.078

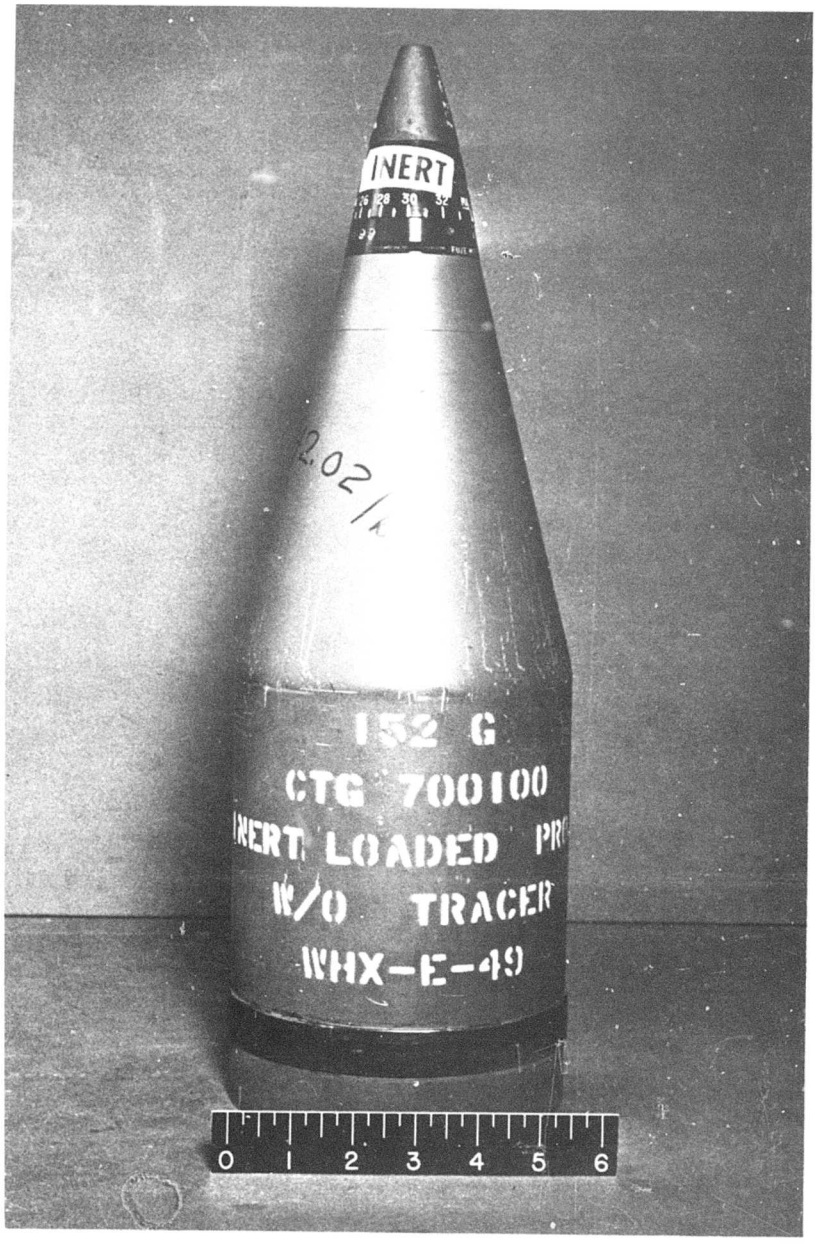

Figure 1. XM617 Projectile

Figure 2. M551 Sheridian Vehicle

XM-617

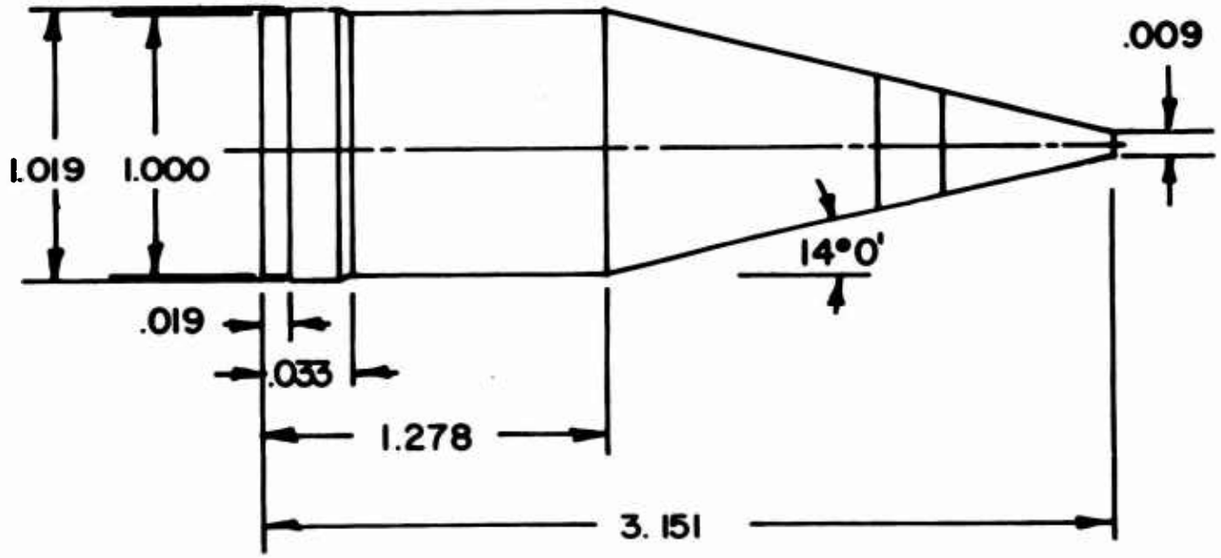

WT.= 19.06 Kg I_x= 459.91 Kg-cm^2
CG= 1.086 (FROM BASE) I_y= 1884.69 Kg-cm^2

NOTE: ALL DIMENSIONS ARE IN CALIBERS

Figure 3. Projectile Schematic

conventional shells of similar caliber; however, its well defined shape makes possible good yaw measurements. The shell is rather light weight for its size and as a result responds more to a given force, yielding a larger than normal swerving motion which is favorable in reducing the normal force coefficient.

The XM617 is a variation of an existing shell shape and the planned testing was basically of a confirmatory nature, thus a coarse net test program was deemed reasonable. The sparseness of the data makes it impossible to draw an exact interpretation throughout the Mach number range covered. This is particularly noticeable in the Mach 1 region. The use of the shell does not inherently involve large yaws and no effort was made to induce yaws larger than were occurring naturally. As a result, a coupling of initial launch conditions and projectile stability produced smaller than desired yawing motions for those rounds launched near Mach 1. In spite of the sparseness of the data and the small motions of some rounds, it is felt that the definition of the data is adequate to describe the behavior of the shell.

Typical range shadowgraphs of the projectile in flight at various Mach numbers are shown in Figures 4 to 9. Because of the projectile's configuration, the flow exhibits local shock waves at the nose-body junction at the lowest test speed of Mach 0.8. However, a fully supersonic flow is not obtained until about Mach 1.3.

A. Drag

A least square fit of time as a cubic in distance was used to obtain C_D for each round. C_D was then reduced to C_{D_o} by the expression:

$$C_D = C_{D_o} + C_{D_{\overline{\delta^2}}} \overline{\delta^2}$$

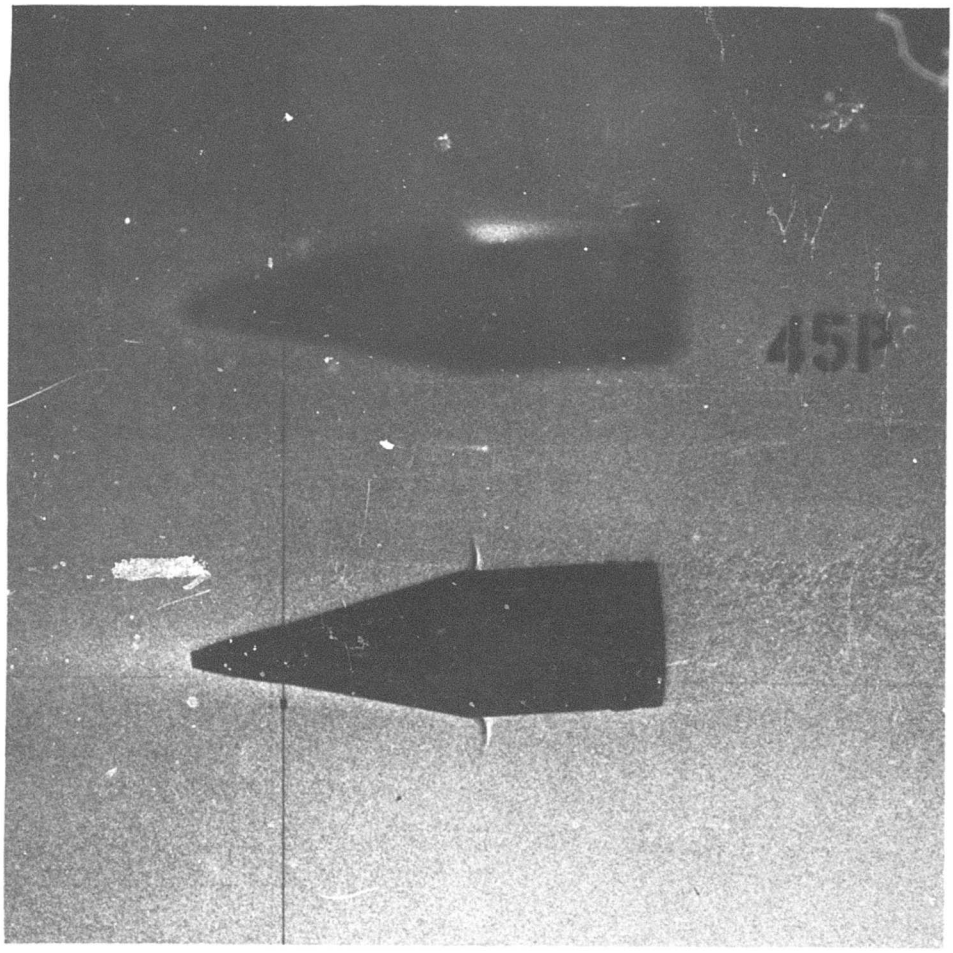

Figure 4. Shadowgraph of XM617, M = 0.87

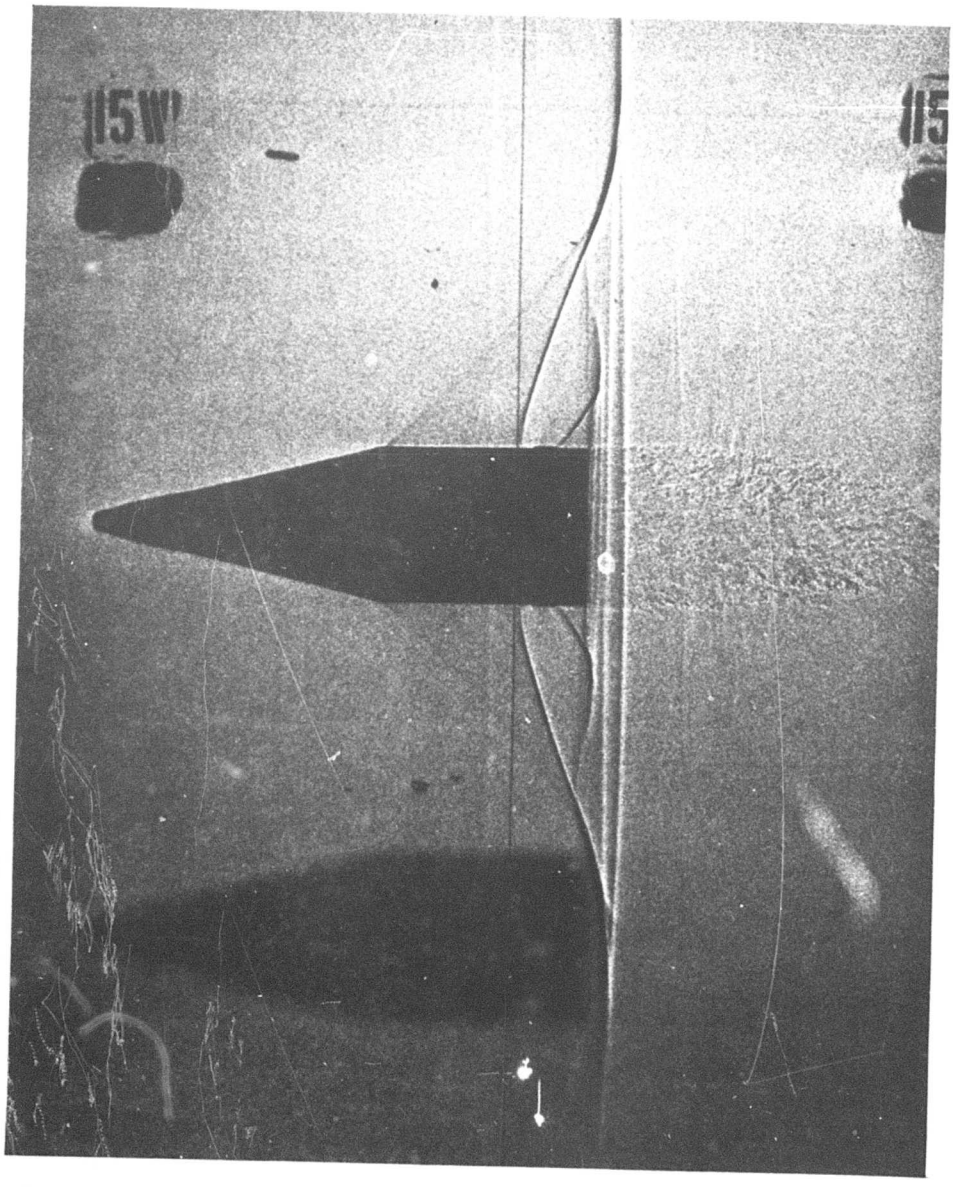

Figure 5. Shadowgraph of XM617, M = 0.95

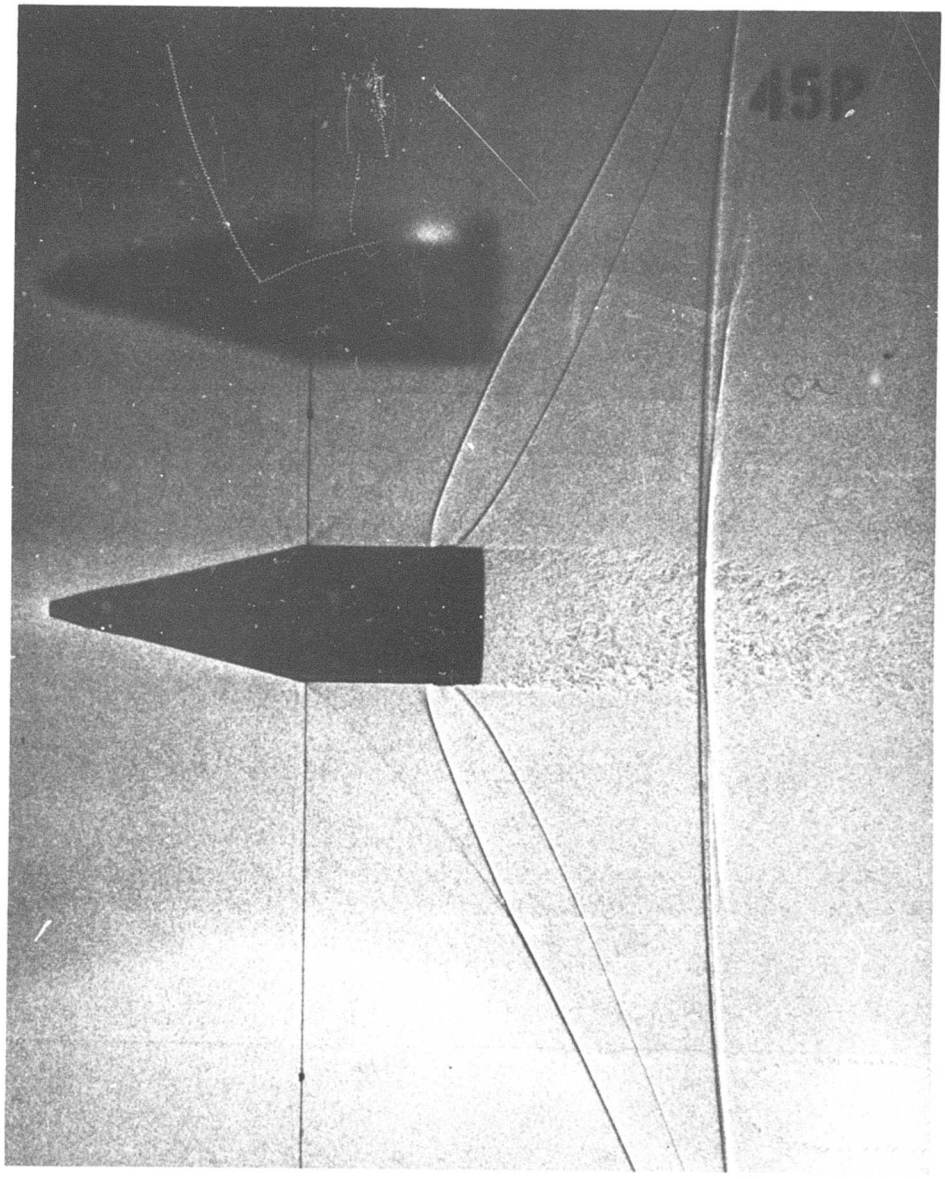

Figure 6. Shadowgraph of XM617, M = 1.00

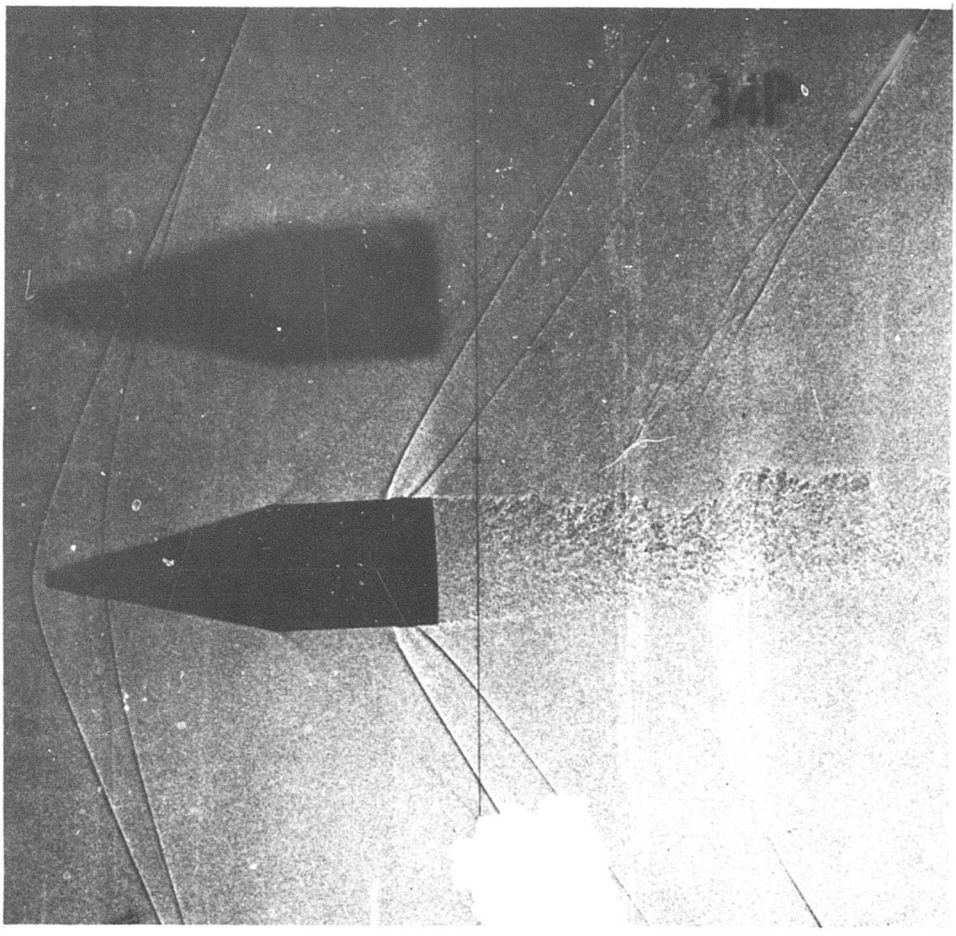

Figure 7. Shadowgraph of XM617, M = 1.15

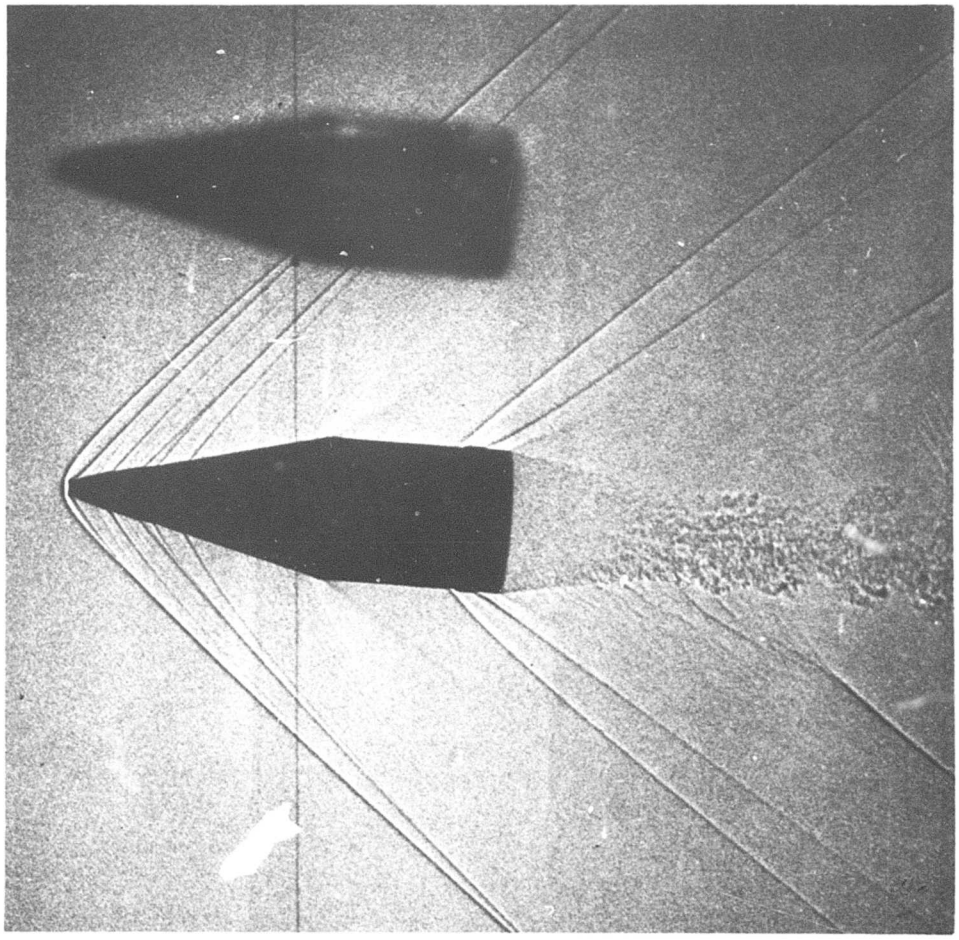

Figure 8. Shadowgraph of XM617, M = 1.42

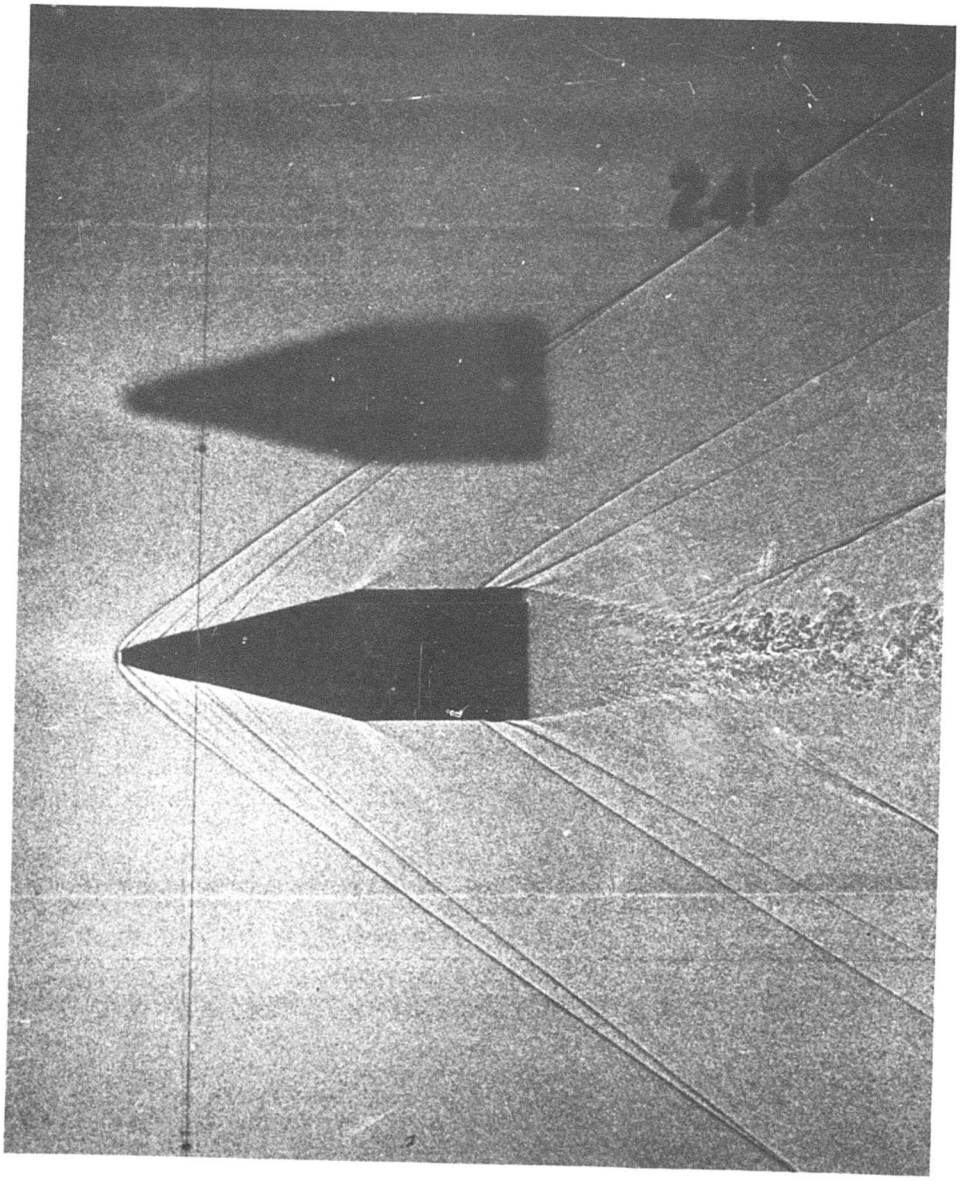

Figure 9. Shadowgraph of XM617, M = 1.83

where $C_{D_{\overline{\delta^2}}}$ is the yaw drag coefficient and $\overline{\delta^2}$ is the mean squared yaw $(K_1^2 + K_2^2)$. $C_{D_{\overline{\delta^2}}}$ was obtained by plotting C_D versus $\overline{\delta^2}$ for a given Mach number and determining the slope of the line. Although the data indicated that $C_{D_{\overline{\delta^2}}}$ was Mach number sensitive, there were insufficient data to determine this effect. Thus, a constant value for $C_{D_{\overline{\delta^2}}}$ of 6.57/rad^2 was used. The zero yaw coefficient, C_{D_o}, is plotted versus Mach number in Figure 10.

Figure 11 shows Figure 10 plotted over data reduced from field firings using information gathered by a modified Hawk radar system. The shaded area is drag data not reduced for yaw effects which were obtained from a large number of rounds, all launched at standard velocity. The sharp tail off of the drag at Mach 1.0 is indicative of ground noise effects as the projectile neared the terminal point of the trajectory. The up-swept portion of the radar data above Mach 1.6 is indicative of increased drag due to yaw induced at launch which then damps to smaller yaw values.

The good agreement shown between the two curves adds confidence for the use of radar techniques to evaluate changes in initial launch conditions due to modification to the gun system.

B. Static Moment, Force and Center of Pressure

The static moment slope C_{M_α} is plotted versus Mach number in Figure 12. The data are quite consistent for the two test rounds at each Mach number and the supersonic portion of the curve is well defined. The portion of the curve below Mach 1.3 reflects only a trend in the data since a more definite interpretation is prohibited because of the sharp variation in C_{M_α} and the coarse data net. There is

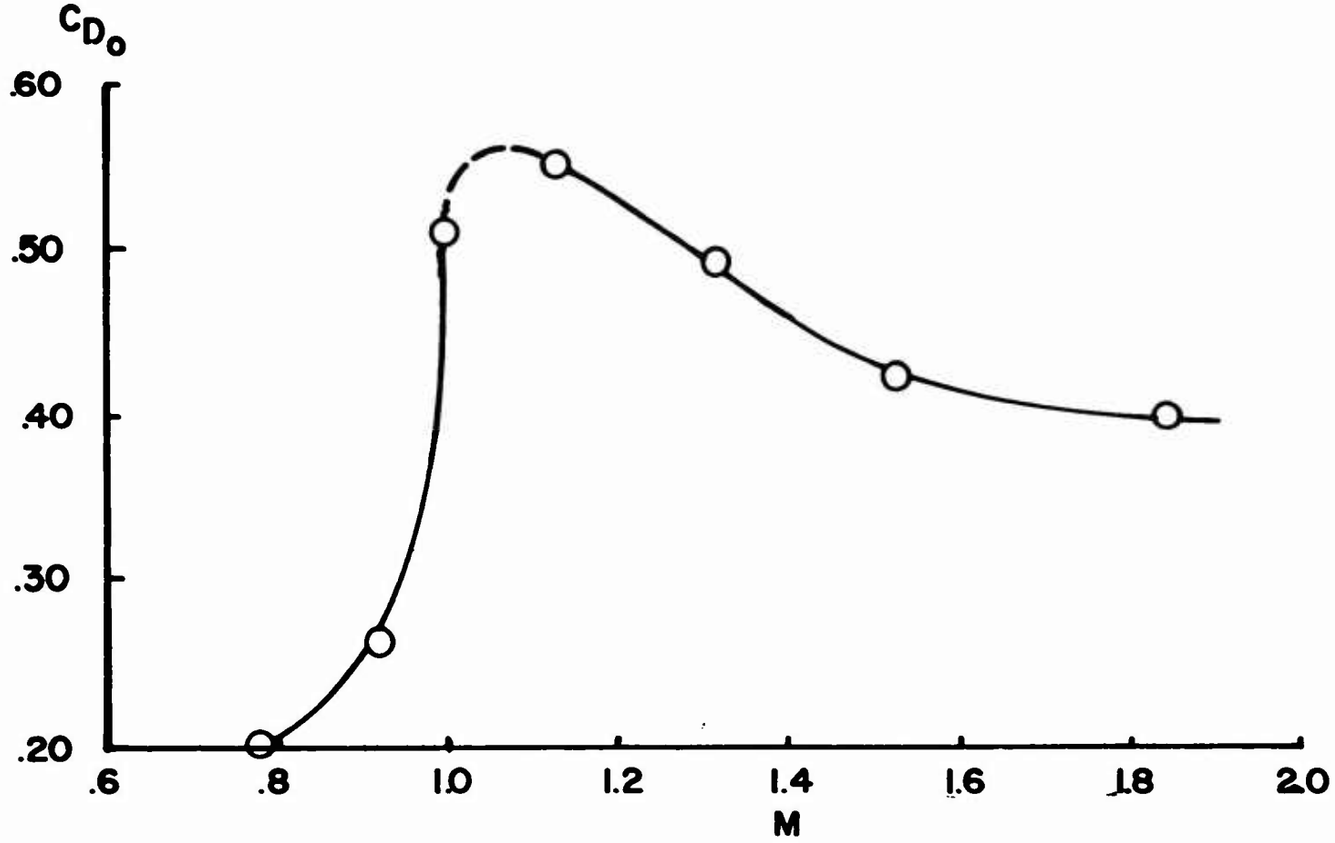

Figure 10. Zero-Yaw Drag Coefficient vs Mach Number

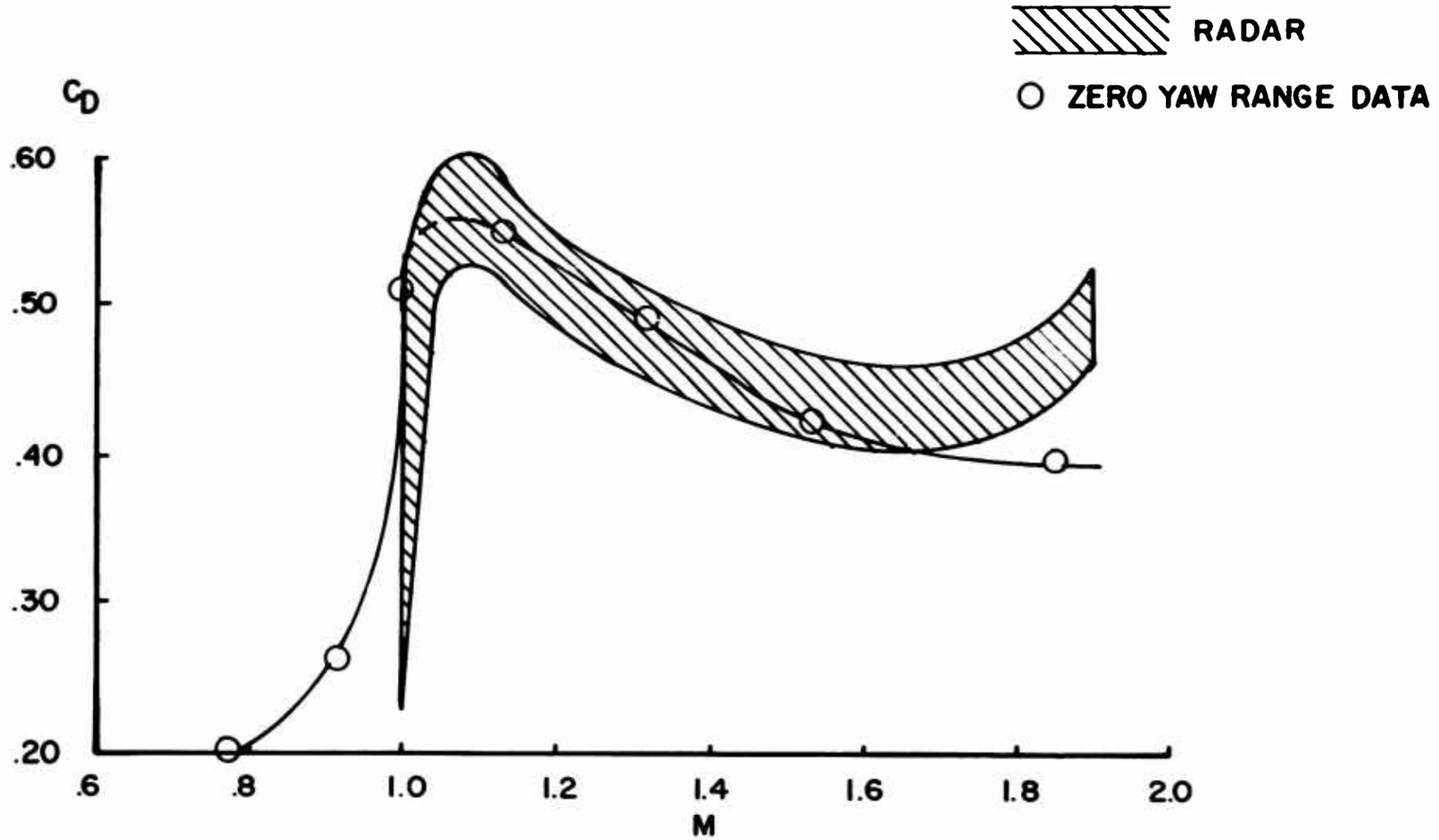

Figure 11. Drag Coefficient vs Mach Number

little variation in the static moment slope from Mach 1.8 to nearly Mach 1 with a value of C_{M_α} remaining between 1.1 and 1.2. Subsonically, the value of C_{M_α} peaks to nearly 150 percent of the supersonic value at about 0.9 where it appears to decrease rapidly for lower Mach number values. Part of the deviation between data points at the same Mach number is caused by a nonlinearity of the moment slope with yaw level which is seen at both subsonic and supersonic speeds by the higher average yaw data having lower C_{M_α} values. There are too few data to attempt a determination of the cubic nonlinear coefficient, however.

The normal force slope C_{N_α} is shown in Figure 13. The supersonic portion is quite flat with an average value of 2.75 followed by a systematic rise as the Mach number decreases from 1.2 to 1.0. There is a sudden drop just below Mach 1 and then a recovery to higher values at lower speeds. The minimum value of the force coefficient coincides with the maximum value of the moment coefficient which indicated a considerable change of the pressure distribution about the body at this Mach number of 0.92.

The center of pressure of the normal force is derived by the relation:

$$C_{M_\alpha} = C_{N_\alpha} (CP_N - c.m.) \quad .$$

Figure 14 is based on the previously discussed curves for the static moment slope and normal force slope, and indicates a center of pressure for the supersonic speeds just aft of 1.5 calibers from the base. A sudden forward movement of about four tenths of the caliber is shown as the Mach number decreases from 1.0 to .9 and then an aft retreat of CP_N as the speed lowers.

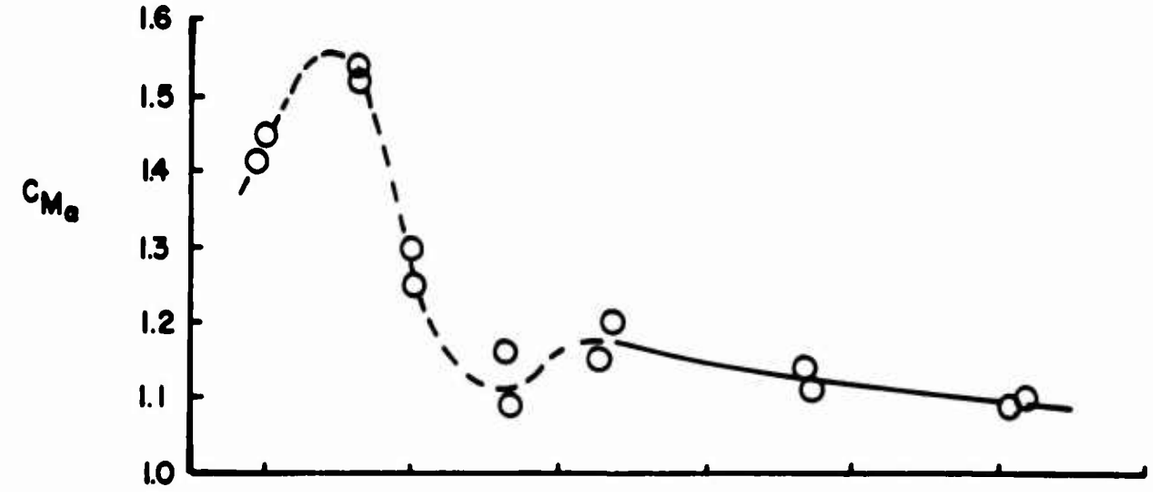

Figure 12. Static Moment Slope vs Mach Number

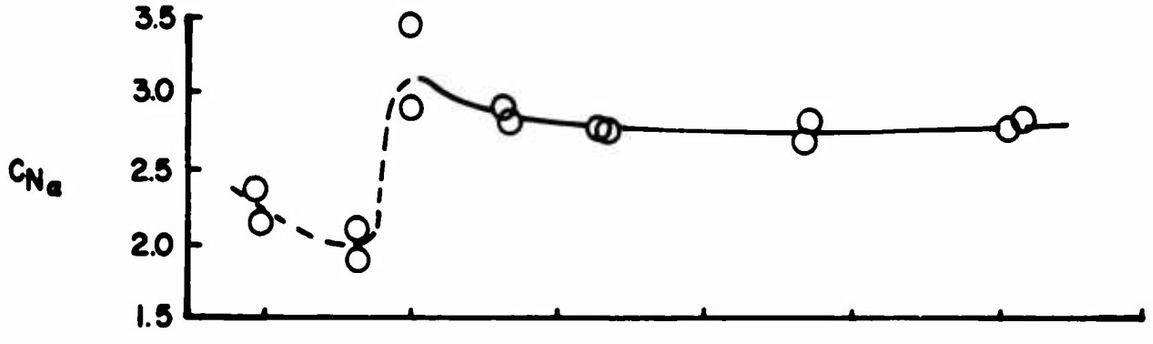

Figure 13. Normal Force Slope vs Mach Number

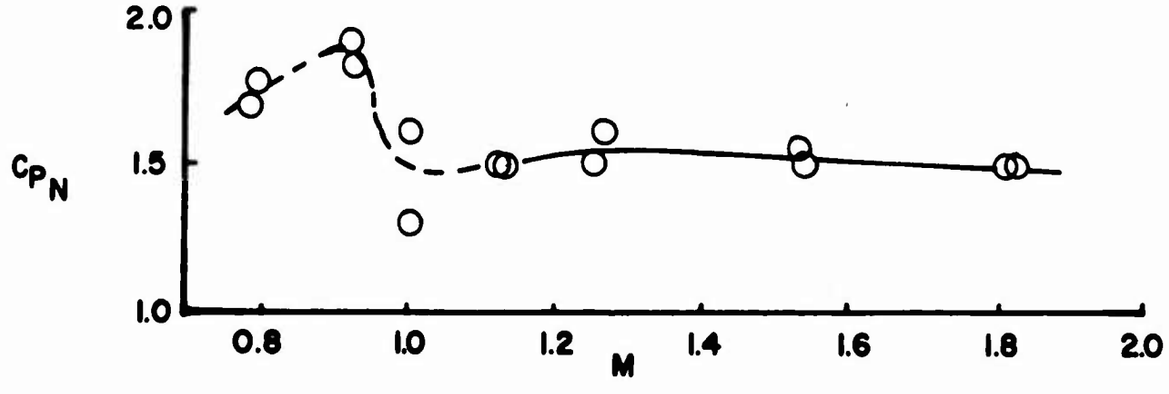

Figure 14. Center of Pressure of Normal Force vs Mach Number

C. Magnus Moment

The Magnus moment slope $C_{M_{p\alpha}}$ is plotted as a function of Mach number in Figure 15. Small positive values are indicated above Mach 1.5 which increase 300 percent as the speed decreases to Mach 1.3. Considerable scatter is evident from Mach 1.3 to below sonic speed. Apart from the fact that these data come from rounds having some of the smallest yaws, hence less accurate results, it is probable that the coarse data net is obscuring a more complicated Mach number variation. Also nonlinearities due to yaw effects which are not defined would increase the apparent scatter. Below Mach 1, $C_{M_{p\alpha}}$ decreases and appears to become negative near the lowest test Mach number of 0.8.

D. Damping Moment

The damping moments for the reduction of the range data are determined in the combination $C_{M_q} + C_{M_{\dot{\alpha}}}$. The plot of this combination versus Mach number is shown in Figure 16. A negative value for the damping moment slope indicates that the contribution is damping. All values determined from the tests are negative, but a decrease in damping is indicated subsonically as the speed decreases.

III. STABILITY AND DAMPING

The stability properties of a shell reflect its aerodynamic properties, its inertial properties and its spin characteristics. The classic stability factor s_g indicates the gyroscopic stability level of the shell and it must remain adequately above a value of one for all use conditions. Although a shell may be gyroscopically stable, a transient yaw disturbance may grow and the shell is dynamically unstable. The damping rates of the precessional and nutational yaw modes

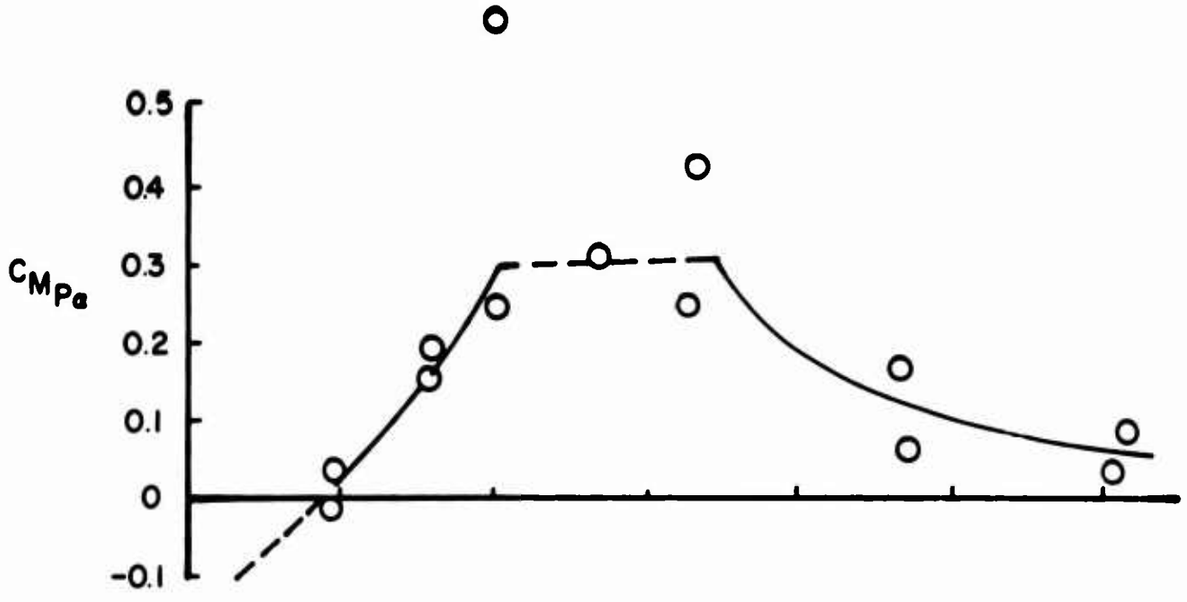

Figure 15. Magnus Moment Slope vs Mach Number

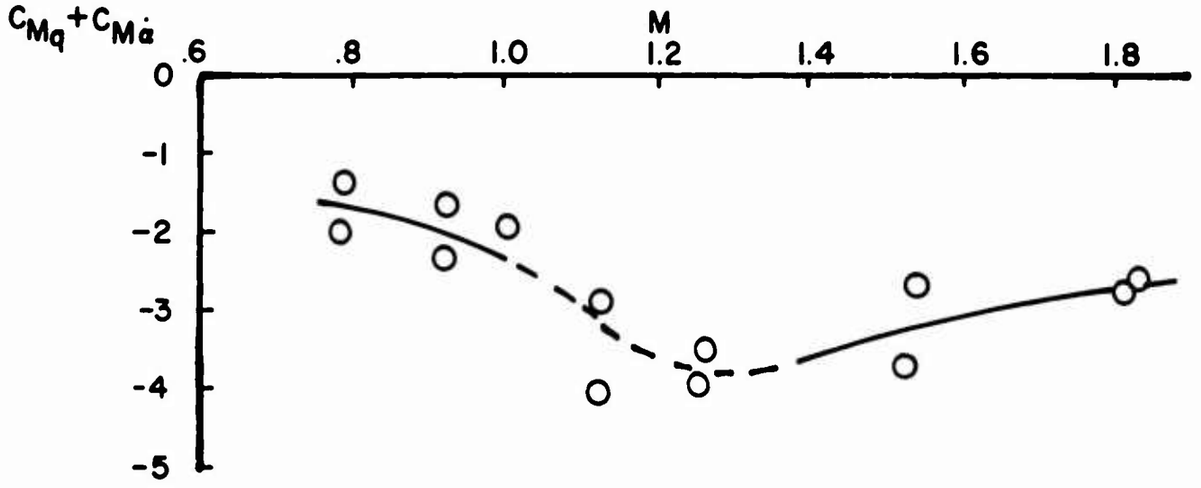

Figure 16. Damping Moment Slope vs Mach Number

show this. Dynamic stability is not as absolute a requirement as is gyroscopic stability. Weak divergence of either mode for a brief time can be tolerated in some cases: none-the-less damping under all conditions is generally more desirable.

The gyroscopic stability and the modal damping rates obtained in ballistic range tests are based on the twist of the launcher. These measurements show well the relative stability level of the shell, but as used the XM617 is launched at one velocity and the lower speeds are attained as the shell slows down along the trajectory. Since the spin decay is usually slower than that for the velocity, the spin to velocity ratio increases over the muzzle value. In order to exhibit the impact of these changes on the stability and damping properties of the shell, three representative trajectories were computed and the spin and velocity variations along the trajectories determined. These conditions and the aerodynamic properties derived from the range tests were then used to compute s_g and the damping rates along the sample trajectories.

A. Gyroscopic Stability

The gyroscopic stability factor s_g is given for small yaw conditions by:

$$s_g = \frac{p^2 I_x^2}{2\rho S \ell V^2 I_y C_{M_\alpha}} \quad .$$

The values obtained in the range tests are plotted as a function of Mach number in Figure 17. The values are determined at essentially the muzzle spin conditions and at the standard velocity the resultant value of s_g is 2.0. The stability factor decreases slightly as the speed decreases until Mach 1.3 where the values then increase rather sharply

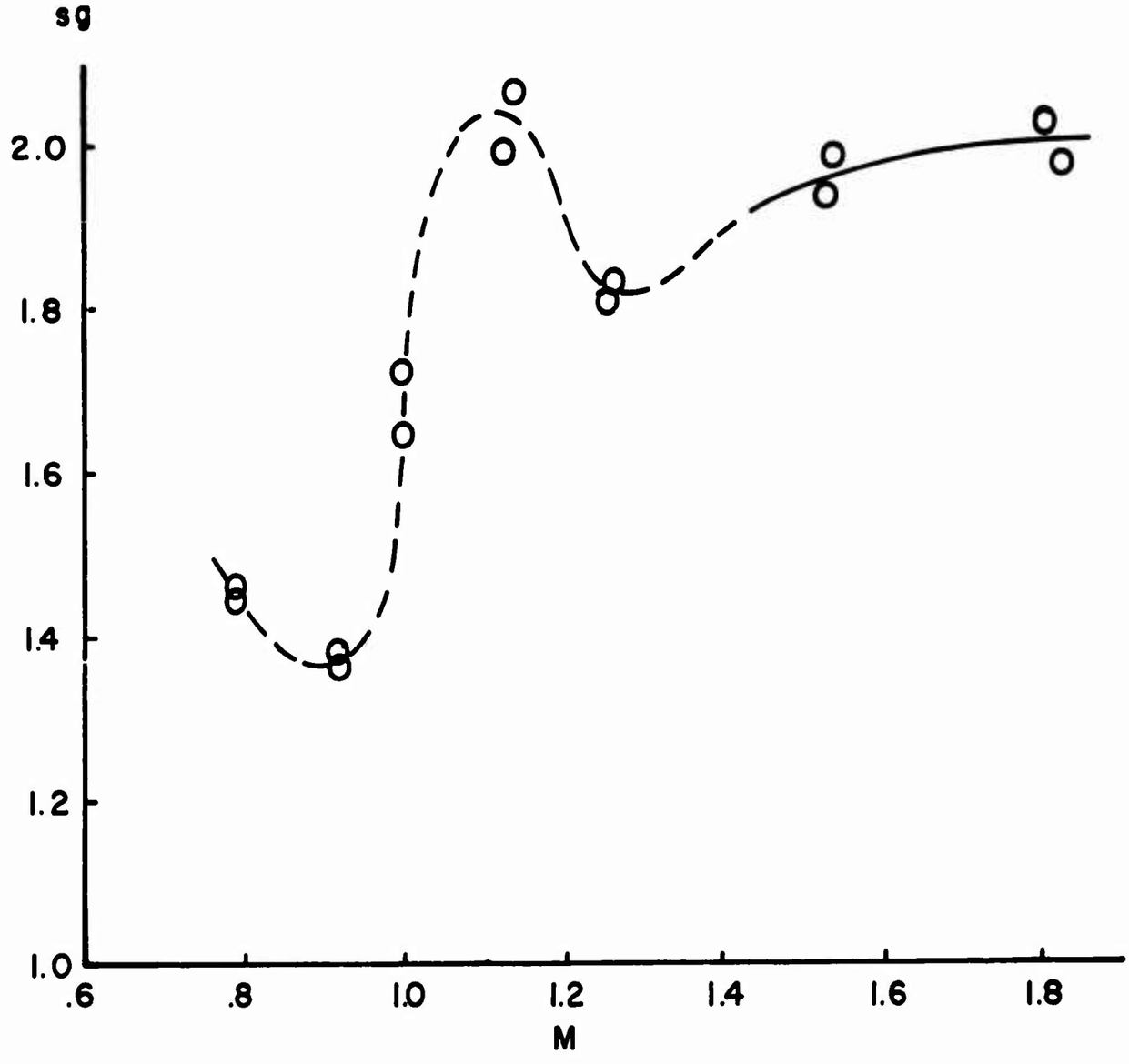

Figure 17. Gyroscopic Stability vs Mach Number

until Mach 1.1. In the range between Mach 1.1 and 0.9 a relative large decrease in the stability factor is indicated, reflecting the peaking of the static moment slope, and a minimum value for s_g of 1.4 is reached. A slight increase in the stability factor is indicated as the speed decreases further.

The relatively low minimum value for the gyroscopic stability at muzzle spin conditions at transonic speeds could be of concern if the shell were used in a zoned system but the concern is not necessarily valid for a projectile launched only at supersonic speed. Computed velocity and spin histories for three typical trajectories are given in Figure 18; the trajectories are for quadrant angles of elevation of 10°, 20° and 35°. The spin appears as one curve on the figure for all three trajectories because the small variations that occur over this range of quadrant angles disappear at the scale of the plot. The spin shows a nearly constant rate of decay while the velocity decreases more rapidly at first due to the combined action of gravity and the high drag at supersonic and transonic speeds. Thereafter the velocity decrease is slower and on the longest trajectory there is even a slight increase in speed of the shell on the terminal part of the downward leg of the trajectory. Figure 19 is a plot of s_g computed as a function of range for the spin and Mach number conditions of these trajectories. The impact of decelerating through sonic speed with the resulting rapid changes in C_{M_α} is still evident but only as a minor change in the general trend of the curves in the vicinity of the 2000 meter range. There is an apparent discrepancy in the value of the stability factor quoted from the range testing, $s_g = 2.0$, and that shown for zero range conditions in the trajectory cases computed, $s_g \doteq 1.8$. This is due to the fact that the center of the data range for the spark

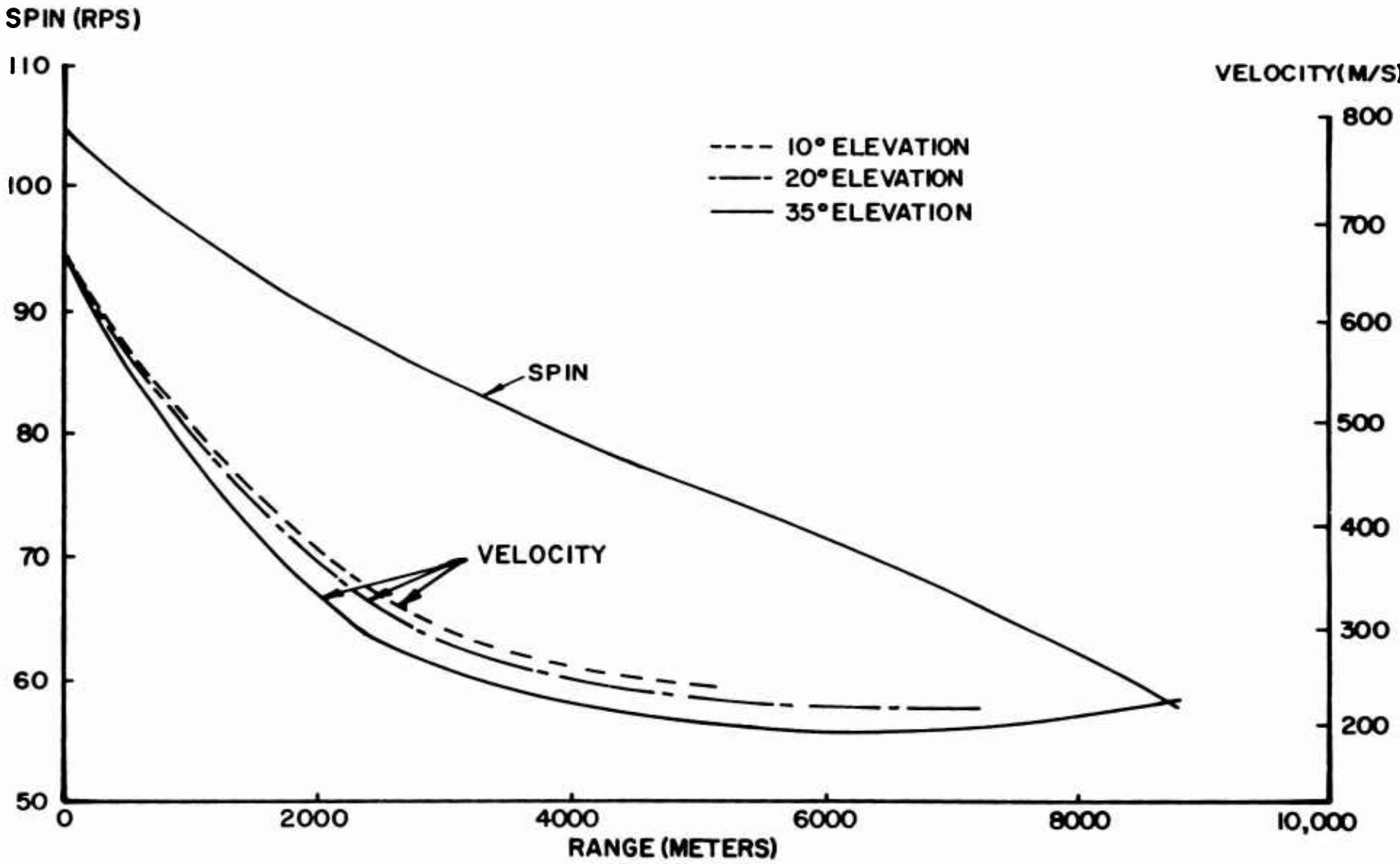

Figure 18. Spin vs Range and Velocity vs Range

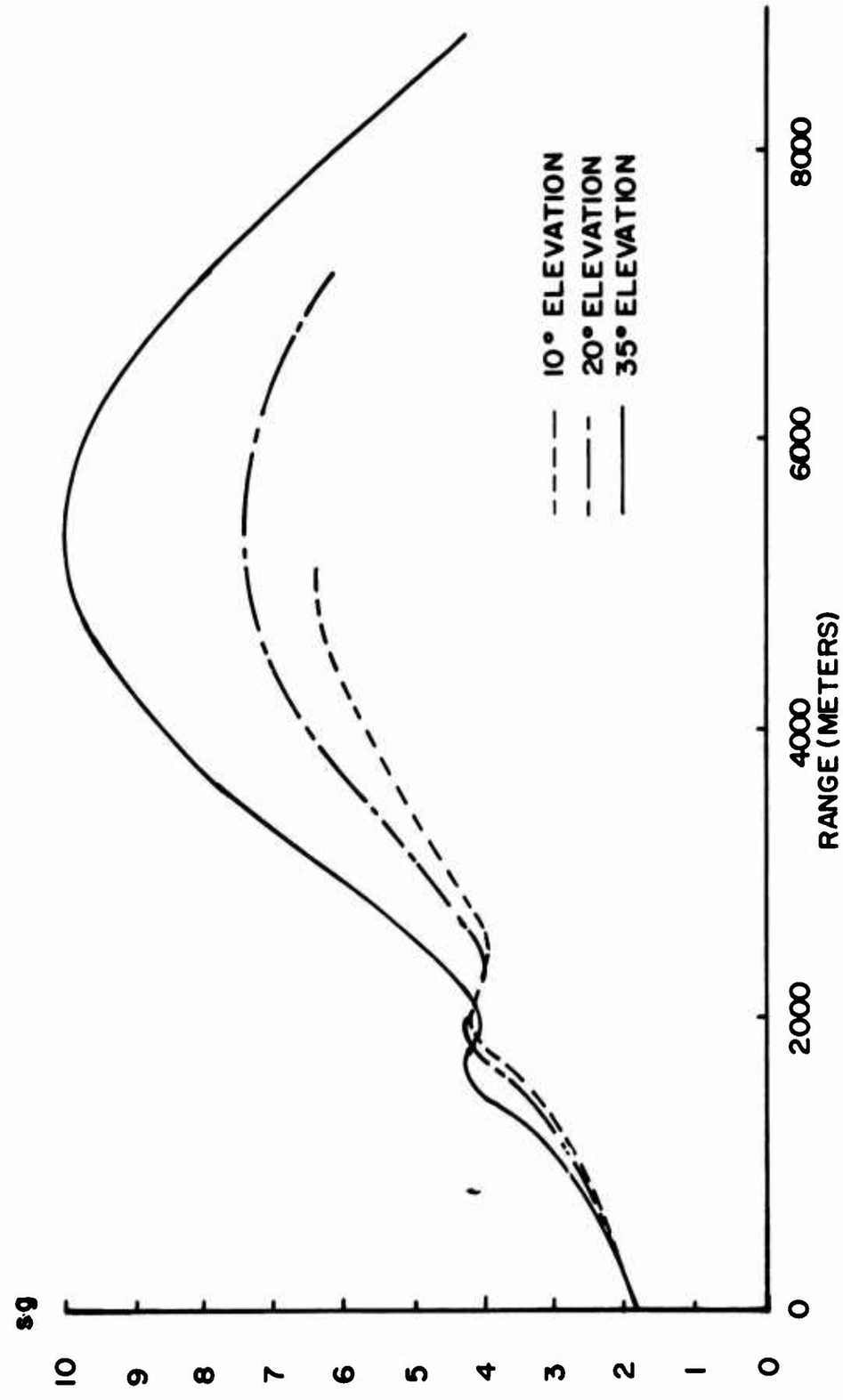

Figure 19. Gyroscopic Stability vs Range

shadowgraphic range tests is actually at about 150 meters range from the gun and despite the fact that the XM617 is a large caliber shell it is ballistically light and there are relatively large changes due to the rapid deceleration even in this short distance. It can be seen from the curves that the trajectory value of the stability factor always exceeds the value at the muzzle condition even for the terminus of the longer range trajectory.

B. Damping Rates

The nutational and precessional damping rates for the range test conditions are plotted as a function of Mach number in Figure 20. Both modes show damping under all test conditions. The precessional damping is smaller, about half that of the nutational in the supersonic region. The only point that is possibly disturbing about the damping rates is that the precessional rate is decreasing markedly between Mach 0.9 and Mach 0.8. The value of the precessional damping at M = 0.8 coupled with the incremental change between Mach 0.9 and 0.8 would extrapolate to a zero damping level between Mach 0.7 and 0.6. Because of the coarse data net and the fact that the flow about the shell is not truly subsonic at Mach 0.8, it is difficult to extrapolate the damping curves with confidence.

To obtain a picture of the damping under actual trajectory conditions, the aerodynamic coefficient curves were used together with the computed velocity and spin conditions from trajectory computations. The Mach number conditions for the trajectory computations do extend slightly below that of the test data, and it was necessary to extrapolate the individual data curves. A comparison of the individual aerodynamic property curves of the XM617 with those obtained from similar shapes allows extrapolation with greater confidence than is possible when extrapolating a

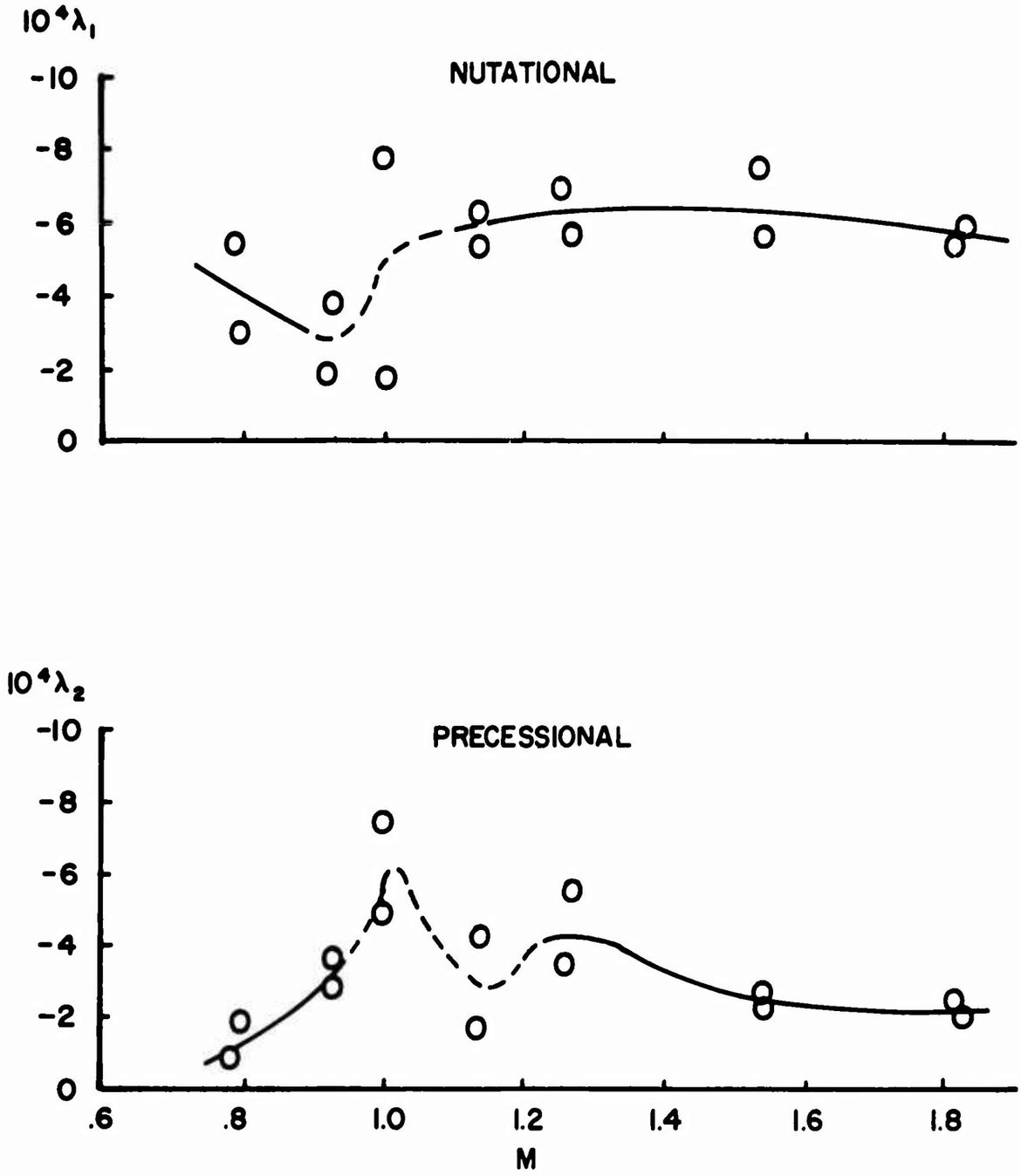

Figure 20. Damping Rates vs Mach Number
(A Negative λ_j Yields Damped Motion)

composite aerodynamic and physical property such as the damping rates. The results are shown in Figure 21. There is not a great deal of difference in the three curves for the various trajectories. The stable nutational mode is always strongly damped while the more critical precessional component shows a sharp decrease in the level of damping at the crossover to subsonic speed. The resultant curves show no tendency to extrapolate to negative damping or divergent values at increased ranges. This result is dependent, of course, on the extrapolation of the various individual data curves, but only a considerable error in the extrapolation of the Magnus moment coefficient $C_{M_{p\alpha}}$ could markedly change the end result.

IV. SUMMARY

The aerodynamic and stability data determined from the range tests of the XM617 are good, but the coarse data net prohibits a detailed interpretation. However, ample data are available to describe the flight behavior of the projectile. The range test data do indicate low gyroscopic stability and weak damping for the subsonic portion of the data; thus, computations were made for some typical real range trajectories. For the conditions considered in the real range trajectories, the stability and damping properties of the projectile were found to be adequate.

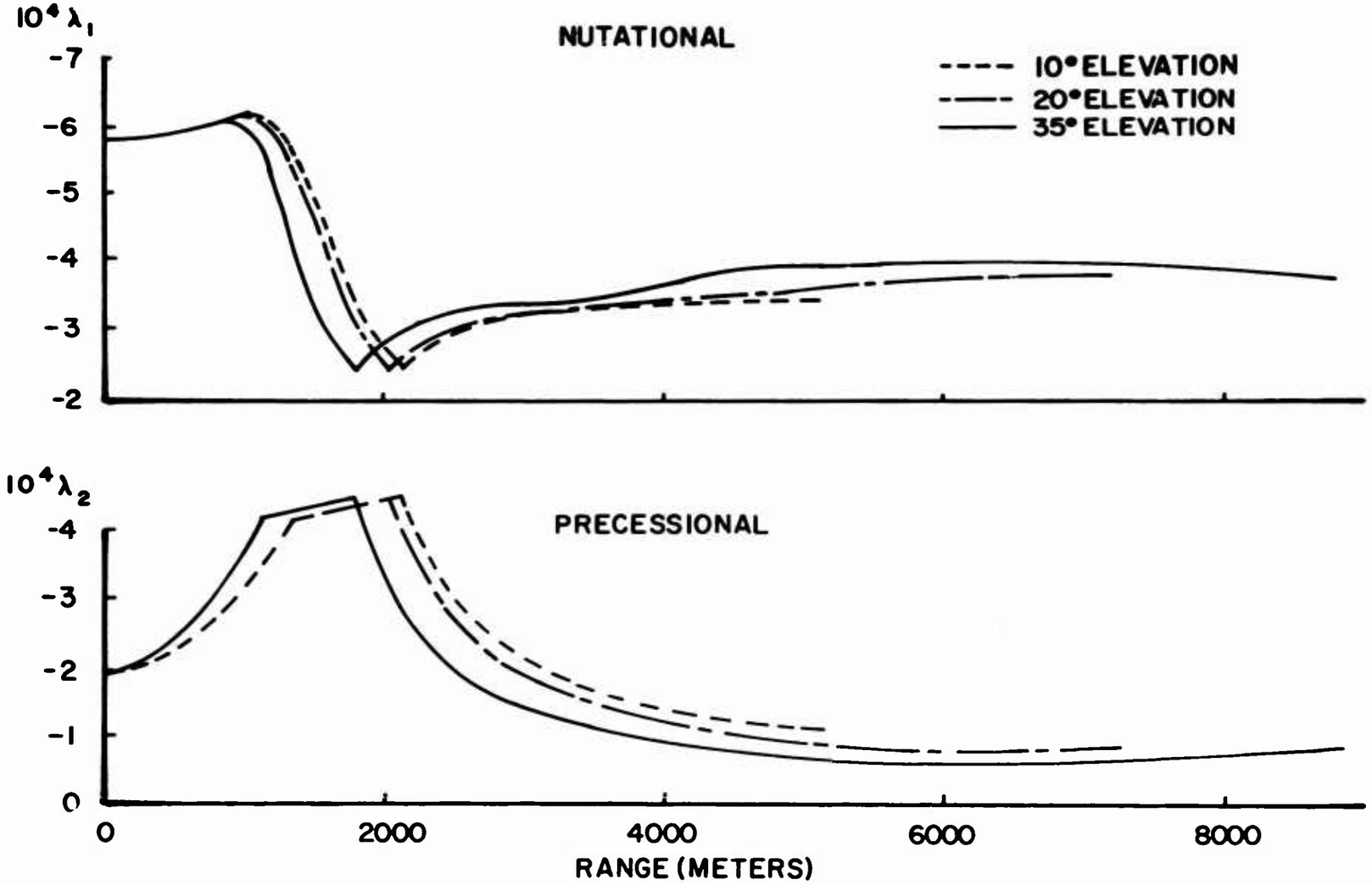

Figure 21. Damping Rates vs Range

REFERENCES

1. W. K. Rogers, Jr., "The Transonic Free Flight Range", Ballistic Research Laboratories Report 1044, June 1958 (AD 200177).

2. E. R. Dickinson, "Physical Measurements of Projectiles", Ballistic Research Laboratories Technical Note 874, February 1954 (AD 803103).

3. C. H. Murphy, "Free Flight Motion of Symmetric Missiles", Ballistic Research Laboratories Report 1216, July 1963 (AD 442757).

4. E. R. Dickinson, "Stability Determination of the 152mm HEAT/MP Shell XM409E4", Ballistic Research Laboratories Technical Note 1404, May 1961. Report is Confidential. (AD 374985L)

5. E. R. Dickinson, "Stability Determination of the 152mm HEAT/MP-T Shell XM409E5 Mod. 2A", Ballistic Research Laboratories Memorandum Report 1391, February 1962. Report is Confidential. (AD 329235)

Unclassified
Security Classification

DOCUMENT CONTROL DATA - R & D

(Security classification of title, body of abstract and indexing annotation must be entered when the overall report is classified)

1. ORIGINATING ACTIVITY *(Corporate author)*
U.S. Army Aberdeen Research & Development Center
Ballistic Research Laboratories
Aberdeen Proving Ground, Maryland

2a. REPORT SECURITY CLASSIFICATION
Unclassified

2b. GROUP

3. REPORT TITLE
AERODYNAMIC PROPERTIES OF THE 152mm XM617 PROJECTILE

4. DESCRIPTIVE NOTES *(Type of report and inclusive dates)*
BRL Memorandum Report

5. AUTHOR(S) *(First name, middle initial, last name)*
Fred J. Brandon

6. REPORT DATE	7a. TOTAL NO. OF PAGES	7b. NO. OF REFS
July 1969	42	5

8a. CONTRACT OR GRANT NO.	9a. ORIGINATOR'S REPORT NUMBER(S)
b. PROJECT NO. RDT&E 1T262301A201	Memorandum Report No. 1998
c.	9b. OTHER REPORT NO(S) *(Any other numbers that may be assigned this report)*
d.	

10. DISTRIBUTION STATEMENT
This document is subject to special export controls and each transmittal to foreign governments or foreign nationals may be made only with prior approval of Commanding Officer, U.S. Army Aberdeen Research and Development Center, Aberdeen Proving Ground, Maryland.

11. SUPPLEMENTARY NOTES	12. SPONSORING MILITARY ACTIVITY
	U.S. Army Materiel Command Washington, D.C.

13. ABSTRACT

The results obtained from exterior ballistic tests of the XM617 projectile are presented and discussed. An XM81E12 launcher with a twist of one turn in 41.2 calibers was used. Some real range drag, stability and damping characteristics are also presented and discussed.

DD FORM 1 NOV 68 1473 REPLACES DD FORM 1473, 1 JAN 64, WHICH IS OBSOLETE FOR ARMY USE.

Unclassified
Security Classification

14 KEY WORDS	LINK A		LINK B		LINK C	
	ROLE	WT	ROLE	WT	ROLE	WT
Aerodynamic Characteristics Artillery Ammunition Range Testing						